Comparative study between supported bimetallic catalysts for nitrate remediation in water

Mouhamad Rachini, Mira Jaafar, Nabil Tabaja, Sami Tlais, Rasha Hamdan, Fatima Al Ali, Ola Haidar, Christine Lancelot, Mohammad Kassem, Eugene Bychkov, et al.

Research Article

Mouhamad Rachini, Mira Jaafar*, Nabil Tabaja, Sami Tlais, Rasha Hamdan, Fatima Al Ali, Ola Haidar, Christine Lancelot, Mohammad Kassem, Eugene Bychkov, Lucette Tidahy, Renaud Cousin, Dorothée Dewaele, Tayssir Hamieh*, Joumana Toufaily*

Comparative study between supported bimetallic catalysts for nitrate remediation in water

https://doi.org/10.1515/chem-2022-0303
received January 5, 2023; accepted February 27, 2023

Abstract: As the population grows and the demand for water rises, the development of efficient and sustainable water purification techniques is becoming increasingly important to ensure access to clean and safe water in the future. The pollution of surface and groundwater by nitrate (NO_3^-) is a growing global concern due to the rise in nitrogen-rich waste released from agriculture and industry. The removal of nitrate ions from aqueous media using bimetallic catalysts loaded on several supports was studied. Multiwalled carbon nanotubes, activated carbon, titanium dioxide, titanium dioxide/multiwalled carbon nanotubes, and Santa Barbara Amorphous-15 were used as supports to synthesize these bimetallic catalysts. The effects of the support type, supported metal, and catalyst reduction method on the nitrate reduction activity in water were investigated. The catalysts were characterized by X-ray diffraction, fourier-transform infrared spectroscopy, Brunauer-Emmett-Teller isotherm, inductively coupled

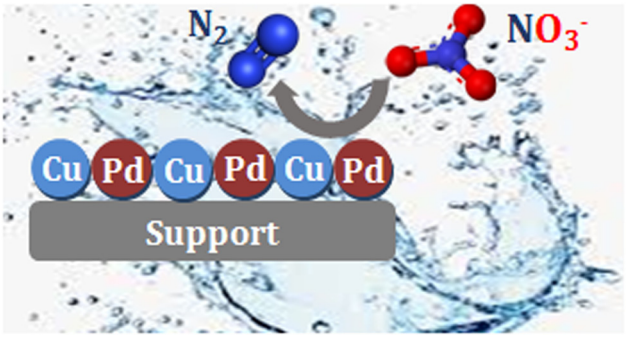

Graphical Abstract

* Corresponding author: Mira Jaafar, Laboratory of Materials, Catalysis, Environment and Analytical Methods (MCEMA), EDST, FS, Lebanese University, P.O. Box 11-2806, Hariri Campus, Hadath, Lebanon; Laboratory of Applied Studies for Sustainable Development and Renewable Energy (LEADDER), EDST, Lebanese University, P.O. Box 11-2806, Hariri Campus, Hadath, Lebanon, e-mail: mira.jaafar@hotmail.fr
* Corresponding author: Tayssir Hamieh, Laboratory of Materials, Catalysis, Environment and Analytical Methods (MCEMA), EDST, FS, Lebanese University, P.O. Box 11-2806, Hariri Campus, Hadath, Lebanon; Faculty of Science and Engineering, Maastricht University, P.O. Box 616, 6200 MD, Maastricht, The Netherlands, e-mail: t.hamieh@maastrichtuniversity.nl
* Corresponding author: Joumana Toufaily, Laboratory of Applied Studies for Sustainable Development and Renewable Energy (LEADDER), EDST, Lebanese University, P.O. Box 11-2806, Hariri Campus, Hadath, Lebanon, e-mail: joumana.toufaily@ul.edu.lb
Mouhamad Rachini: Laboratory of Materials, Catalysis, Environment and Analytical Methods (MCEMA), EDST, FS, Lebanese University, P.O. Box 11-2806, Hariri Campus, Hadath, Lebanon; Université du Littoral Côte d'Opale (ULCO), LPCA, EA 4493, F-59140 Dunkerque, France; Laboratory of Applied Studies for Sustainable Development and Renewable Energy (LEADDER), EDST, Lebanese University, P.O. Box 11-2806, Hariri Campus, Hadath, Lebanon
Nabil Tabaja, Rasha Hamdan: Laboratory of Materials, Catalysis, Environment and Analytical Methods (MCEMA), EDST, FS, Lebanese University, P.O. Box 11-2806, Hariri Campus, Hadath, Lebanon; Laboratory of Applied Studies for Sustainable Development and Renewable Energy (LEADDER), EDST, Lebanese University, P.O. Box 11-2806, Hariri Campus, Hadath, Lebanon
Sami Tlais: College of Engineering and Technology, American University of the Middle East, Kuwait City, Kuwait
Fatima Al Ali: Laboratory of Applied Studies for Sustainable Development and Renewable Energy (LEADDER), EDST, Lebanese University, P.O. Box 11-2806, Hariri Campus, Hadath, Lebanon
Ola Haidar: Laboratory of Applied Studies for Sustainable Development and Renewable Energy (LEADDER), EDST, Lebanese University, P.O. Box 11-2806, Hariri Campus, Hadath, Lebanon; Department of Chemistry, American University of Beirut, P.O. Box 11-0236, Riad El-Solh, Beirut 1107 2020, Lebanon
Christine Lancelot: Université de Lille – Centrale Lille/ENSCL, UCCS, Villeneuve d'Ascq, 59655, France
Mohammad Kassem, Eugene Bychkov: Université du Littoral Côte d'Opale (ULCO), LPCA, EA 4493, F-59140 Dunkerque, France
Lucette Tidahy, Renaud Cousin: Université du Littoral Côte d'Opale, UCEIV, Unité de Chimie Environnementale et Interactions sur le Vivant, EA 4492, SFR Condorcet FR CNRS 3417, Dunkerque, France
Dorothée Dewaele: Centre Commun de Mesures, Université du Littoral Côte d'Opale, Dunkerque 59140, France

plasma spectroscopy, and field emission gun scanning transmission electron microscope. In terms of nitrate conversion, high-temperature hydrogen reduction of the catalysts was a more effective method of catalyst preparation than $NaBH_4$ reduction. Except for the carbon nanotube-TiO_2 composite, pH fixation using CO_2 flow improved the efficiency of supported catalysts. The catalysts 1Pd–1Cu/TiO_2 and 1Pd–Cu/SBA-15 presented the highest catalytic activity, but the latter was the most selective to nitrogen.

Keywords: nitrate reduction, bimetallic catalyst, SBA-15, carbon nanotubes, TiO2, activated carbon, XRD, BET, SEM, FTIR

1 Introduction

The worldwide nitrogen cycle has changed altogether over the past 200 years. Pollution from the excessive use of nitrate is the major disrupter of this natural cycle. Nitrate enters the environment through various human activities, such as agricultural and urban activities, the use of pesticides, improper disposal and dumping of industrial waste, etc. Nitrate is highly soluble in water and readily enters groundwater reservoirs and nearby water systems. At a concentration above 50 mg/L, nitrate causes many health complications such as methemoglobinemia, diabetes, and the spread of infectious diseases [1]. Aquatic systems with high concentrations of nitrate and weak buffering capacity may suffer from water acidification due to the generation of nitric acid by the nitrate reductase in freshwater, compromising the survival of acid-sensitive fish and other aquatic biota. In addition, in open water systems, nitrate promotes eutrophication, impairing aquatic life's ability to breathe [2].

Nitrate nondestructive treatment methods, such as electrodialysis, ion exchange, and reverse osmosis, produce residual streams with high nitrate concentrations that require proper disposal [3–7]. The commonly used nitrate-destructive treatment method, biological denitrification, produces water that necessitates deep postdisinfection and waste sludge that needs to be dealt with [8–10]. Another promising nitrate destructive treatment method is catalytic reduction. The absence of posttreatment requirements and sludge production, along with energy and space-saving, are advantages of catalytic reduction over the previously stated methods. Studies have shown that nitrates can be reduced effectively using bimetallic catalysts supported on active or passive materials, but this releases byproducts such as nitrite and ammonia [11]. These byproducts are more hazardous to human health than nitrates. The World Health Organization sets a maximum limit of 10 ppm for nitrates, but even lower limits of 0.03 and 0.4 ppm for nitrites and ammonium, respectively. The main challenge in making the catalytic reduction of nitrates competitive is to develop innovative catalysts and configurations to increase nitrogen selectivity [3,11–13].

Numerous studies have been conducted on the reaction mechanism of nitrate reduction over supported bimetallic catalysts utilizing hydrogen as the reducing agent [14]. Based on the earlier work of Vorlop and Tacke [5], using a bimetallic system (preferably Pd–Cu) promotes the adsorption of nitrate [5]. After adsorption, nitrate is first reduced to nitrite; nitrite is preconverted to other intermediate products (NO and N_2O). Ultimately, nitrogen is formed as the main product, and the long-sided ammonium is an undesirable by-product of overhydrogenation [15]. Prüsse and Vorlop [13] proposed a mechanistic model involving three main elements: 1) nitrate reduction mainly occurs at bimetallic (Pd–Cu; Pd–Sn) sites, 2) nitrite reduction occurs at monometallic (Pd) sites, and 3) the reaction selectivity is determined by the N/reductant ratio of a single metal site of palladium. As per Deganello et al., the nitrite reduction activity of bimetallic catalysts decreased with the increasing promoter metal content [16], a conclusion supported by the abundant formation of nitrite during nitrate reduction. Later, Ilinitch et al. [17] proposed an 18-step mechanism for nitrate reduction over supported Pd–Cu bimetallic catalysts. However, the most widely accepted mechanism is that of Epron et al. [18]. They suggested that the promoter metal reduces NO_3^- through redox reactions, while the noble metal (Pd or Pt) activates hydrogen to reduce the promoter metal. Although noble metals do not appear to be active in reducing NO_3^-, they are very active in decomposing nitrite (this is believed to be due to the presence of active hydrogen) [18,19]. Bimetallic catalysts usually consist of a noble metal (mainly Pd or Pt, but also Ru, Rh, or Ir) and a promoter metal (such as Cu, Sn, Ag, Ni, Fe, or In) deposited on different supports. Pd–Cu, Pd–Sn, and Pt–Cu appear to be the most effective combination, but the metals alone are not selective enough for nitrogen [20,21]. To increase their selectivity, they are usually deposited on supports. Many support materials have been used, including alumina [13,22–24], silica [25,26], titania [27], activated carbon (AC) [26–29], carbon nanotubes (CNTs) [30,31], ceria [32], tin oxide [33], polymer [34], zirconia [35], and aluminum oxide film [36,37].

Several reasons behind catalyst deactivation have been reported, including surface fouling of the catalyst surface, promoter irreversible oxidation, and decomposition of the bonding between the catalyst and the support [38].

Furthermore, catalyst deactivation is aggravated in the presence of other ions and pollutants. Metal impregnation and metal aggregation during the catalyst preparation are among the reasons that affect the catalyst reactivity and N_2 selectivity. Catalyst support appears to influence all the aforementioned issues.

The fundamental objective of this work is to screen classical supports: titanium oxide (TiO_2) and AC along with newly developed supports such as CNTs and mesoporous silica materials SBA-15 for different bimetallic catalysts (Pd–Cu, Pt–Cu, and Pd–Sn) in the reduction of nitrates and the production of nitrogen. The active phase of the catalysts, which is responsible for catalyzing the reaction, was prepared using various methods ($NaBH_4$ vs H_2 reduction, at 100°C vs 200°C). The physico-chemical, textural, and compositional characterizations of the supported catalyst were then evaluated using different analytical techniques (X-ray diffraction (XRD), fourier-transform infrared spectroscopy (FTIR), Brunauer-Emmett-Teller (BET) isotherm, inductively coupled plasma spectroscopy (ICP), and scanning electron microscope (SEM)) to determine the structure and the composition of the materials. Finally, the efficiency of the supports was tested to determine their catalytic activity in reducing nitrate selectively into nitrogen gas.

2 Experimental

2.1 Materials

SBA-15 (Santa Barbara Amorphous-15) synthesized at our laboratory three types of CNTs, which differ between them by properties: CNT1 (specialty multiwalled) SMW 210; ≥98% carbon-based, O.D. × I.D. × L: 10 nm ± 1 nm × 4.5 nm ± 0.5 nm × 3–~6 μm), CNT2 (NA.230; >90% carbon-based, D × L: 110–170 nm × 5–9 μm), and CNT3 (Nanocyl 3100; <5% metal oxide followed by thermogravimetric analysis, 9. 5 nm × 1.5 μm) were purchased from Sigma-Aldrich. AC originated from Fluka Analytical, and titanium oxide (Titania, TiO_2) Degussa P25, purchased from Sigma-Aldrich, were used as supports. TiO_2 and AC were used as received. However, the multiwalled carbon nanotubes (MWCNTs) were purified and functionalized [39,40] before use in some experiments. Nitric acid (69%), palladium chloride (99%), platinum(II) chloride (99.9%), tin(II) chloride (98%), tetraethyl orthosilicate, reagent grade 98 in weight%, poly-block (oxyethylene) – blockpoly (oxypropylene) – block-poly (oxyethylene) triblock copolymer Pluronic, P123, of molecular weight 5,800 g/mol, copper nitrate (99%), sodium nitrate (≥99%), sodium borohydride (≥96%), and titanium isopropoxide Ti $(OC_3H_7)_4$ purchased from Sigma-Aldrich were used in the preparation of the bimetallic supported catalysts. Acetonitrile (99.85%) from Scharlau was used as the solvent. While chloroform (99.0–99.4%), potassium sodium tartrate tetrahydrate (99%), sodium salicylate (99.5%), and sulfuric acid (98%), purchased from Sigma-Aldrich, and sodium hydroxide (99%), purchased from Riedel-de Haën, were used in the nitrate coloration. Hydroxide pellets originated from UNI-CHEM, ammonium chloride, sodium nitroprusside, and phenol were purchased from Sigma-Aldrich for the ammonia coloration.

2.2 SBA-15 synthesis

In an open container, 500 mL of ultrapure water is acidified with 79.36 mL of HCl (37%). Then, 16.69 g of the precursor "P123" was dissolved in the acidic solution. P123 is a tri-block polymer (PEOPPO-PEO). The thermostat attached to the reactor was set at 35°C, and the solution was kept under mechanical stirring. After the complete dissociation of P123, a clear solution was obtained. Then 39 mL of "TEOS" silica source was added slowly to the solution using a graduated burette.

Immediately after the addition of TEOS, stirring was stopped, and the temperature was maintained at 35°C for 24 h, keeping the container open to evaporate the ethanol that was formed. Afterward, the solution was transferred to a sealed polypropylene container and hydrothermally treated at 130°C for 33 h. Then, it was cooled to room temperature. The solid material was recovered through Buchner filtration, washed three times with ultrapure water, and dried overnight at room temperature for 24 h. The resulting white powder was then calcined at 500°C in an oven with a heating rate of 2°C/min for 6 h [41].

2.3 Catalyst Preparation

In this work, the following supports were used: SBA-15, titanium oxide (TiO_2), AC, and three types of CNTs (CNT1, CNT2, and CNT3). All the supports were used as received without modification, except for the CNTs, which were sometimes functionalized with 8.0 M HNO_3 before metal impregnation functionalized carbon nanotubes (FCNT).

In addition, the MWNTC/TiO_2 composite was prepared using an acid-catalyzed sol–gel method from an alkoxide precursor. The preparation was performed at

room temperature as follows: First, 1.86 mL of $Ti(OC_3H_7)_4$ was dissolved in 12.6 mL of ethanol. The solution was magnetically stirred for 30 minutes, and then we added 0.1 mL of nitric acid. The mixture was coated and kept under constant stirring until a homogeneous gel was formed. The gel was matured in the air for a few days, and the subsequent xerogel was ground into a fine powder. The CNT/TiO_2 composite catalyst was produced using a CNT/TiO_2 weight ratio of 1:5, and the CNT/TiO_2 composite catalyst was calcined under vacuum at 550°C.

In this work, two methods for support preparation were used:

Method 1: Reduction by $NaBH_4$

The catalysts were first prepared by co-impregnating each support in a mixture of ultrapure water and acetonitrile (V/V, 3:1) with $PdCl_2$ or $PtCl_2$ and $Cu(NO_3)_2$ or $SnCl_2$ in the required amounts to obtain the following bimetallic catalysts: 1 wt% Pd–1 wt% Cu, 4 wt% Pd–1 wt% Cu, 1 wt% Pt–1 wt% Cu, and 1 wt% Pd–1 wt% Sn. Then an excess amount of $NaBH_4$ was added dropwise to the solution. After sonication at 65°C for 1 h, the mixture was filtered and washed several times with ultrapure water to completely remove any remaining reducing agents; finally, the solid filtrate was dried at room temperature for 5 days under vacuum.

Method 2: Reduction by thermal treatment under H_2

The catalysts were also prepared by co-impregnating each support in ultrapure water, only this time with $PdCl_2$ and $Cu(NO_3)_2$ in the required amounts to obtain 1 wt % Pd–1 wt% Cu catalyst. After sonication at 65°C for 1 h, the mixture was filtered and washed several times with ultrapure water. Finally, the solid filtrate was dried at room temperature for several days under vacuum and then reduced at 100 or 200°C for 3 h under an H_2 gas flow after being calcinated for 1 h under an N_2 gas flow. In Table 1, the prepared catalysts are listed with the conditions of preparation.

Table 1: The prepared catalysts and their preparation conditions

Catalyst	Preparation method	Reduction temperature (°C)
4Pd–1Cu/FCNT1	1	—
4Pd–1Cu/FCNT2	1	—
2Pt–1Cu/FCNT2	1	—
2Pd–1Sn/FCNT2	1	—
2Pd–1Cu/FCNT2	1	—
1Pd–1Cu/FCNT2	1	—
1Pd–1Cu/FCNT3	1	—
1Pd–1Cu/CNT3	1	—
4Pd–1Cu/AC	1	—
4Pd–1Cu/TiO_2	1	—
4Pd–1Cu/SBA-15	1	—
1Pd–1Cu/SBA-15	2	200
1Pd–1Cu/FCNT3	2	200
1Pd–1Cu/TiO_2	2	200
1Pd–1Cu/CNT3-TiO_2	2	200
1Pd–1Cu/AC	2	200

2.4 Catalyst characterization

The XRD diffractometer was used to identify the crystal phase and the purity of the supports in this study, as well as to detect the presence of deposited metals. The XRD patterns were recorded using a Bruker D8 Advance diffractometer in the reflection mode, with a Cu Kα (35 kV, 30 mA) radiation wavelength of 0.154056 nm and a count time of 2 s/step in the 2θ range of 5–80° with 0.02° increments. The surface area and isotherms were measured through N_2 adsorption using the multipoint BET method on a Micromeritics ASAP 2420 analyzer. The morphology of the supports was characterized using field emission gun scanning transmission electron microscope electron microscopy on a JEOL JSM7100F instrument. The chemical bonds and functional groups of the different supports were analyzed using the Jasco FT/IR-6300. The Pd and Cu content of the catalysts and their distributions were determined using energy-dispersive spectroscopy (EDS) on an EDAX SDD operating at 20 kV and equipped with an SDD Apollo X detector. Metal loading for some catalysts was measured by ICP-OES (ICAP 6300DUO, Thermo). The temperature programmed reduction (TPR) experiments were performed with an Altamira Instrument type an AMI-200 apparatus; samples (150 mg) to 600°C. H_2 consumption was monitored using a thermal conductivity detector and mass spectrometer (Dymaxion 200 amu, Ametek).

2.5 Nitrate reduction

To evaluate the catalytic activity of the nitrate reduction reaction in water, a glass reactor equipped with a magnetic stirrer and gaseous hydrogen and carbon dioxide inlet, capable of generating a reducing atmosphere and fixing the pH at approximately 5.5 at room temperature and atmospheric pressure, was used. Some reduction experiments were performed at approximately constant pH (5.5) using different catalysts (with CO_2 flow), while

other catalysts are tested in the reduction of nitrates without pH fixation (without CO_2 flow) for comparison. In a typical run, 25 mg of catalyst was loaded into a reactor containing 50 mL of sodium nitrate $NaNO_3$ solution (30 mg/L NO_3^-) in demineralized water and the reactor was continuously stirred using an H_2 stream as a reducing agent and CO_2 as a buffer solution in some cases. To measure nitrates converted and nitrites or ammonium formed at the end of the reaction, the solution was filtered through a 0.45 µm micro-filter and analyzed by UV and sometimes by ion chromatography (IC) (Hitachi Elite Lachrom, auto sampler 2200) for the kinetic study.

The selectivities for nitrite, ammonium, and nitrogen are calculated as follows:

$$S_{NO_2^-} = \frac{n_{NO_2^-}}{n_{NO_3^-\ i} - n_{NO_3^-}}, \quad (1)$$

$$S_{NH_4^+} = \frac{n_{NH_4^+}}{n_{NO_3^-\ i} - n_{NO_3^-}}, \quad (2)$$

$$S_{N_2} = \frac{n_{N_2}}{n_{NO_3^-\ i} - n_{NO_3^-}}, \quad (3)$$

where $n_{NO_3^-\ i}$ is the initial amount of nitrate, and $n_{NO_3^-}$, $n_{NO_2^-}$, and $n_{NH_4^+}$ are the amount of each species at the end of the reaction. The measures of nitrogen (n_{N_2}) were determined by a mole balance.

2.6 Adsorption

For the comparison with catalytic reduction, adsorption experiments are carried out with some supports and supported catalysts under the same conditions of catalytic reduction in the absence of H_2 to assess the support adsorption capacity despite the catalytic activity.

2.7 Determination of nitrate and ammonium concentrations by UV-Vis

At the end of the reduction experiments, the nitrate and ammonium concentrations in water treated with different catalysts were determined using a visible spectrophotometer. The following reagents were used to color the nitrate for visible spectroscopic analysis: sodium hydroxide, potassium sodium tartrate solution, and sodium salicylate solution. The absorbance is measured at a wavelength of 415 nm.

The following reagents were used for the detection of ammonium by the mean of visible spectroscopic analysis: chlorinated solution (sodium hydroxide pellets + sodium citrate dihydrate + sodium hypochlorite), solution of sodium nitroprusside and phenol. The absorbance is measured at a wavelength of 630 nm.

3 Results and discussion

3.1 Catalyst characterization

Figure 1 shows the XRD patterns of CNT1, CNT2, AC, and TiO_2, and the patterns of the two types of CNTs CNT1 and CNT2 are almost similar and both show typical peaks at 25.9° and 42.7°, corresponding to the (002) and (100) planes of graphite [42], respectively, indicating a pristine structure. The typical peaks at 24 and 42° in AC correspond to the (002) and (100) planes of AC [43,44], and their widths indicate that AC is in an amorphous state. Two phases can be seen in the TiO_2 pattern, which can be assigned to TiO_2 (anatase (80.5%) and rutile (19.5%)) [45,46]. The XRD small angle pattern (0–4° 2θ) of the SBA-15 sample is shown in Figure 2. The typical XRD pattern of SBA-15 has three characteristic peaks relative to the (100), (110), and (200) planes at 2θ of 0.96, 1.6, and 1.9°, respectively. These peaks characterize the two-dimensional hexagonal structure of SBA-15 [47], which is consistent with SBA-15 synthesized using TEOS as the silica source. So far, SBA-15 material has been successfully synthesized.

Figures 3 and 4 show the XRD patterns of the FCNT1 (after functionalization), 4Pd–1Cu/FCNT1, and FCNT2, 4Pd–1Cu/FCNT2. The CNTs patterns in this two figures have typical peaks at 25.9 and 42.7°, corresponding to

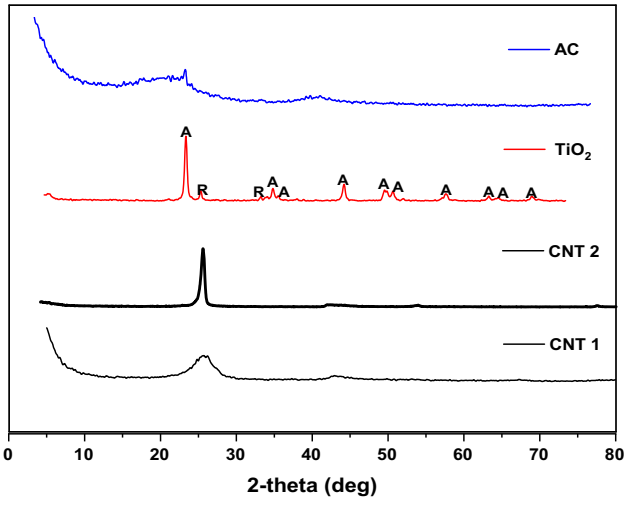

Figure 1: XRD patterns of CNT2, TiO_2, CNT1, and AC.

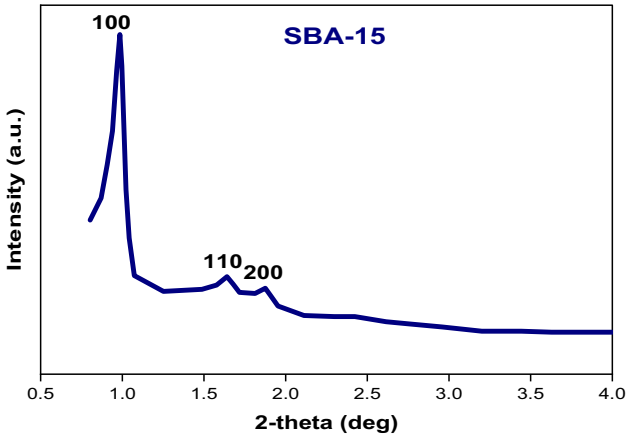

Figure 2: XRD small angle pattern of SBA-15.

the graphite (002) and (100) planes [42], respectively, indicating a pristine structure. There are also peaks at 40.1 and 46.7° corresponding to the reflection planes (111) and (200), respectively, of crystalline Pd with a face-centered cubic (fcc) structure [48]. However, there is no distinct peak that can be attributed to Cu, which would be expected to appear at 43°, which corresponds to the reflection of the (111) plane. This may be due to the low copper content and/or by overlapping with the graphite peak at 42.7°. The same results for Pd and Cu are shown in Figure 5, which shows the XRD patterns of AC and 4Pd–1Cu/AC, and Figure 6 shows the XRD patterns of TiO_2 and 4Pd–1Cu/TiO_2.

The surface modification of MWCNTs by HNO_3 solution was studied by FT-IR to detect the presence of surface functional groups of MWCNTs. The FT-IR results of

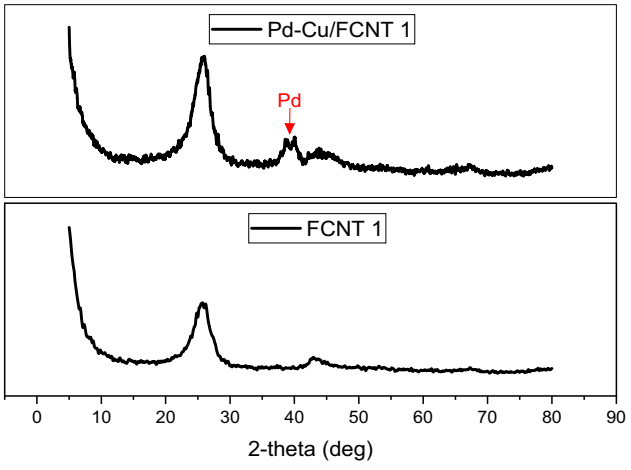

Figure 3: XRD patterns of FCNT1 and 4Pd–1Cu/FCNT1.

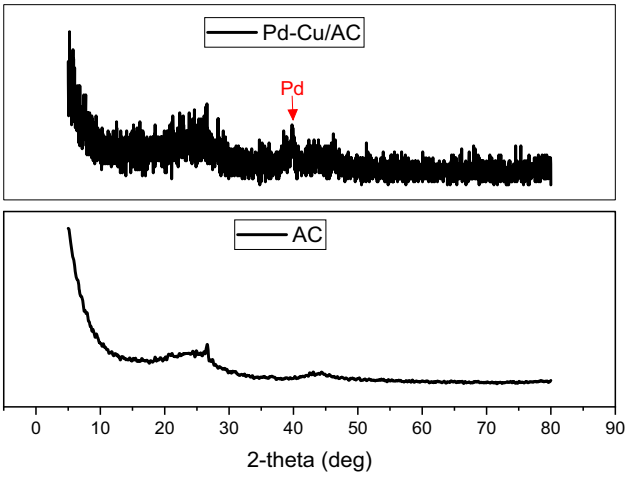

Figuree 5: XRD patterns of AC and 4Pd–1Cu/AC.

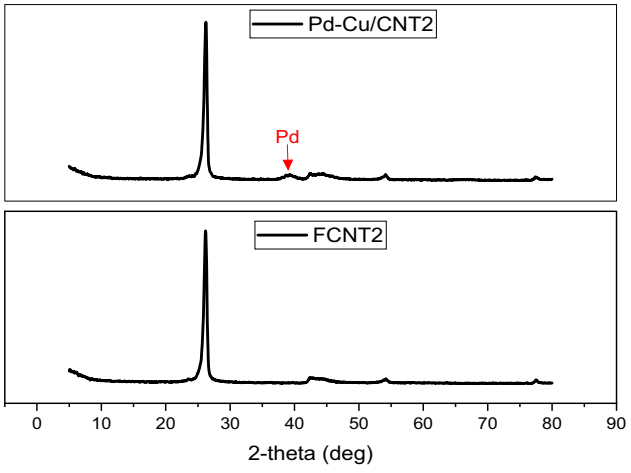

Figuree 4: XRD patterns of FCNT2 and 4Pd–1Cu/FCNT2.

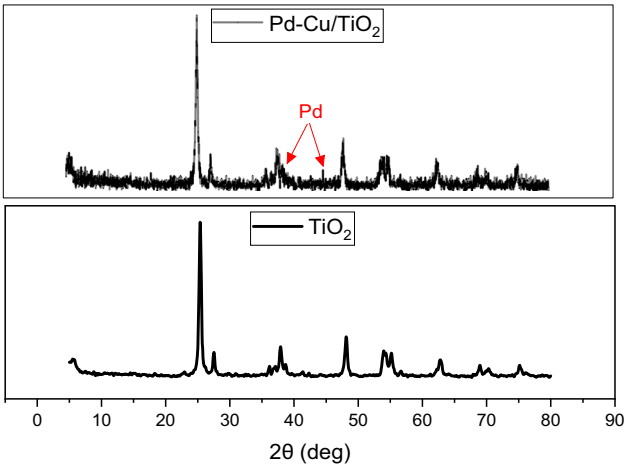

Figuree 6: XRD patterns of TiO_2 and 4Pd–1Cu/TiO_2.

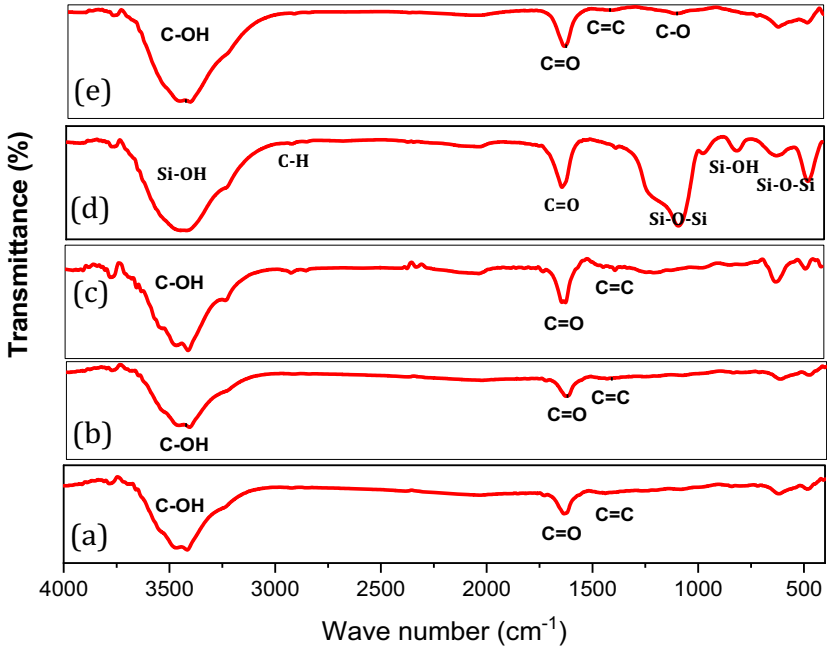

Figure 7: FT-IR: (a) FCNT1, (b) CNT1, (c) CNT3, (d) SBA-15, (e) AC.

FCNT1, CNT1, CNT3, SBA-15, and AC are shown in Figure 7; the same peaks are noticed in the spectra of the CNTs: the peak at 1,430 cm^{-1} can be assigned to an asymmetric C═C stretch [49], while the C–OH stretch is located at 3,430 cm^{-1}, and the nearby C═O double bond is found to have a stretch of 1,710 cm^{-1}. The peaks at 1,710 and 3,430 cm^{-1} correspond to the C═O and OH hydroxyl groups of the carboxylic acid. Thus, we can confirm the presence of these groups even before oxidation with HNO_3. In the FT-IR spectrum of AC, the peak at 3,440 cm^{-1} is assigned to the O–H stretching vibration of the hydroxyl group; the band at 1,700 cm^{-1} is assigned to the C═O stretching vibration of the ketone, aldehyde, lactone, or carboxyl group; and the broadband at 1,000–1,300 cm^{-1} is assigned to C–O stretching in acid, alcohol, phenol, ether, and ester groups; The FT-IR spectrum of the calcined SBA-15 sample shows the absorption bands at 1,082 and 800 cm^{-1} belong to the asymmetric and symmetrical extensions of the Si–O–Si framework, respectively. The strong band at 3,456 cm^{-1} and the weak band at 965 cm^{-1} represent the stretching and bending modes of Si–OH, respectively [50]. The presence of small absorption peaks corresponding to the C–H stretching mode (2,852 and 2,926 cm^{-1}) and bending mode (1,384 cm^{-1}) of the triblock copolymer was also observed [51]. The band at 1,636 cm^{-1} is assigned to the stretching vibration of the carboxyl group (C═O). This indicates that a small amount of surfactant is still present in the sample after calcination.

Figure S1 in the supplementary information shows the FT-IR results of FCNT1, CNT1, and Pd–Cu/FCNT1, and it can be noted that there is no big difference between the three results.

The SEM images of the as-received CNT1, CNT2, and CNT3 are shown in Figure 8. CNTs are of cylindrical shape with nanometric diameter and micrometric length can be seen in the as-received CNTs. We can see clearly the active metals deposited on the surface of the nanotubes in the case of 4Pd–1Cu/CNT2 (Figure 8d and e).

Figure 9 shows the SEM images of titanium dioxide, SBA-15, 1Pd–1Cu/SBA-15, and AC. The surface morphology of TiO_2 (Figure 9c) shows a uniform distribution of nanoscale spherical TiO_2 particles. The AC image shows micron-sized particles (Figure 9d). At this magnification, the surface of the AC is often filled with irregular cavities that can act as primary channels connecting the inner and outer surfaces of the AC, which are not well resolved. SEM images show clearly visible supported active metals on SBA-15 (Figure 9b).

Table 2 summarizes the BET surface area and total pore volume of the supports used in this study before and after impregnation of Pd–Cu metals. AC and SBA-15 media have the two highest BET surfaces. CNT2 has the lowest specific surface area among CNTs and among all other substrates (11 m^2/g), but CNT1 has the largest specific surface area and the largest pore volume among the three types of CNTs, and titanium dioxide exhibits a low

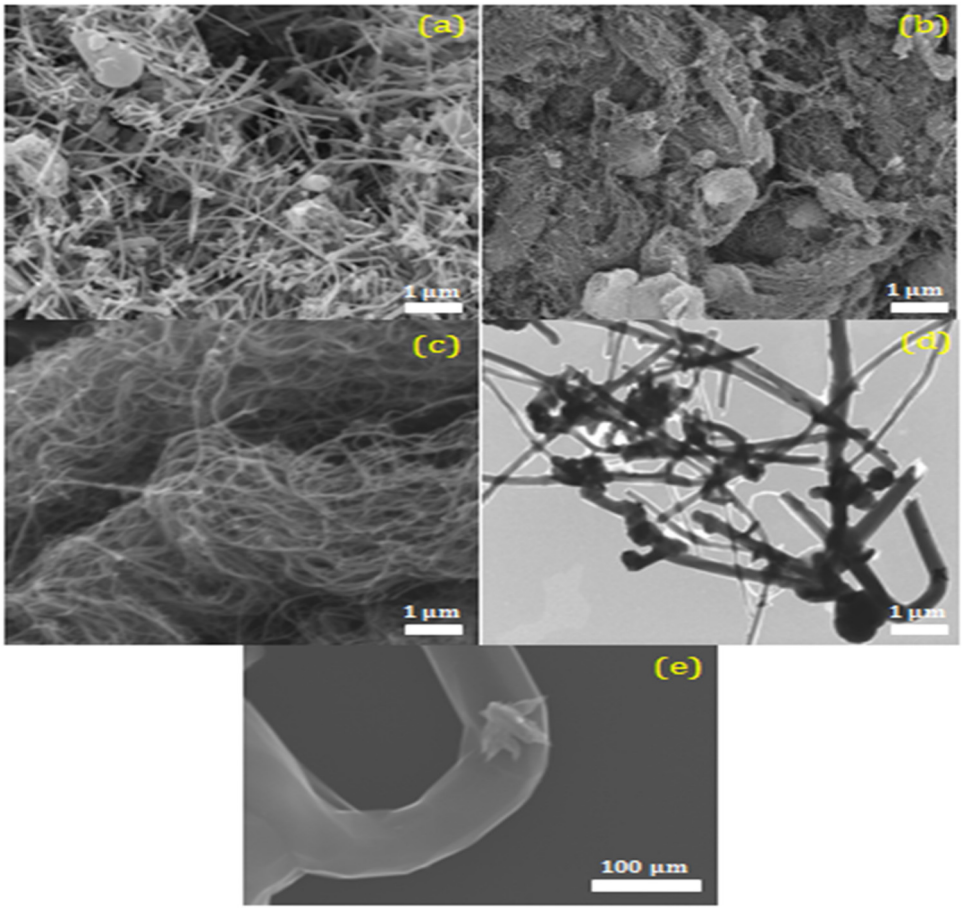

Figure 8: SEM images: (a) CNT2, (b) CNT1, (c) CNT3, (d) and (e) 4Pd–1Cu/CNT2.

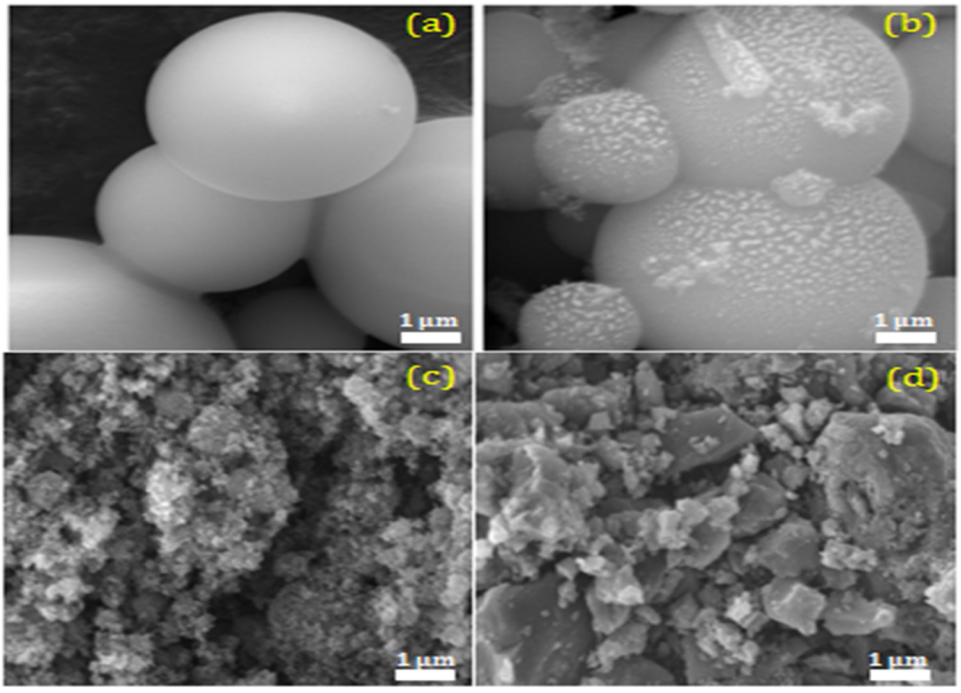

Figure 9: SEM images: (a) SBA-15, (b) 1Pd–1Cu/SBA-15, (c) TiO_2, and (d) AC.

Table 2: BET properties of the used catalysts

Sample	BET surface area (m^2/g)	V_{total} (cm^3/g)
SBA-15	699	0.985
4Pd–1Cu/SBA-15	686	1.09
1Pd–1Cu/SBA-15	684	1.07
AC	977	0.51
4Pd–1Cu/AC	837	0.5
TiO_2	54	0.5
4Pd–1Cu/TiO_2	53	0.5
CNT1	198	1.003
FCNT1	250	1.59
FCNT2	11	N. D.
FCNT3	186	0.405
CNT3	197	1.284
CNT3-TiO_2	95	0.105

BET surface area. In cases where metals are deposited on the surface of the supports, it can be seen that the BET surface area decreases a little (Pd–Cu/SBA-15, Pd–Cu/AC, and Pd–Cu/TiO_2).

To study the specific surface area of the samples, N_2 adsorption–desorption isotherms were performed. The CNT1, CNT3, and TiO_2 isotherms (Figures S2a,b and S3a) belong to type IV, characteristic of mesoporous materials formed by finite multilayers, followed by capillary condensation. Meanwhile, the AC isotherm (Figure S3b) belongs to type I, which is the characteristic of microporous materials. The hysteresis loops of CNTs and TiO_2 are close to H1 type, which corresponds to materials with cylindrical pore geometry and high pore size uniformity. In AC, however, the hysteresis loops are of H4 type, characterized by slit-like pores. In addition, Figure S3c shows the results of nitrogen adsorption–desorption analysis of SBA-15 with a good hysteresis and the adsorption isotherms correspond to type IV [52]. At 0.78, the nitrogen adsorption varies greatly, which is attributed to the capillary condensation of nitrogen through the mesopores. This phenomenon is known as the change that occurs when there is a uniform distribution of the pore size [53].

EDS was used to provide qualitative and semi-quantitative information on the elemental composition of the catalyst surface. The EDS spectra of 4Pd–1Cu/CNT1, 4Pd–1Cu/CNT2, 4Pd–1Cu/AC, and 4Pd–1Cu/TiO_2 are presented in Figures 10–13, respectively. The results show that Pd and Cu are present on the surfaces of these catalysts.

4Pd–1Cu/CNT1 catalyst was chosen to study its TPR profile before its reduction under H_2 to select the appropriate reduction temperature for the bimetallic catalyst and to study the effect of the temperature on the catalyst activity. The result is shown in Figure S4. The reduction peaks attributed to Pdβ-hydride decomposition were observed around 60°C [54,55], which may indicate that Pd is not well dispersed on the support [56]. 4Pd–1Cu/CNT1 catalyst shows a reduction peak in the range of 140–200°C, which can be attributed to the reduction of copper oxides [54,56]. The presence of palladium leads to a decrease in the reduction temperature of copper in bimetallic catalysts, which indicates that intimate contact between copper and palladium species is achieved [56].

Table 3 summarizes the measured ICP results of active metal loading for some selected catalysts. The results show that the loaded metal values differ from the nominal values in most catalysts except in the case

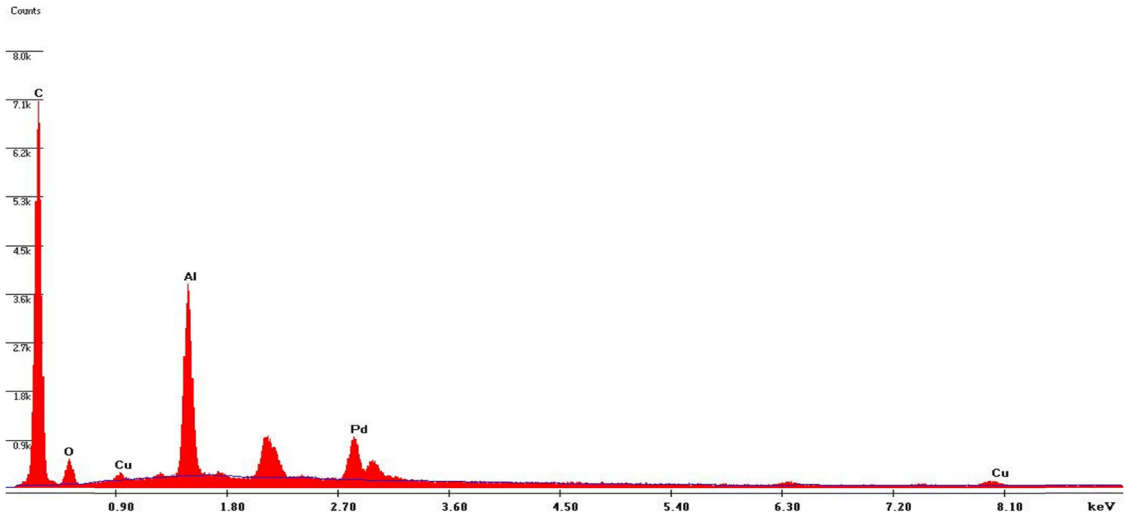

Figure 10: EDX pattern of 4Pd–1Cu/CNT1.

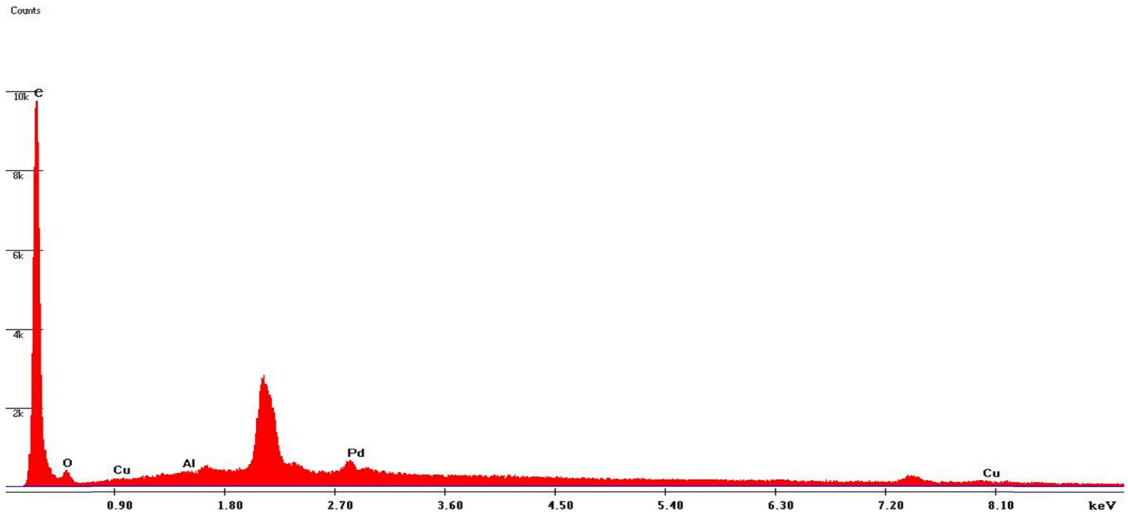

Figure 11: EDX pattern of 4Pd–1Cu/AC.

of 4P–1Cu/TiO_2 and 4P–1Cu/SBA-15 prepared by method 1, and in the case of 1Pd–1Cu/SBA-15 and 1Pd–1Cu/FCNT3 prepared by method 2 at 200°C, where the deposited metal percentage is close to the set values. In the case of 4Pd–1Cu/AC prepared by method 1, 1Pd–1Cu/AC prepared by method 2, and 2Pd–1Sn/CNT2 prepared by method 1, the transition metal is not loaded; this can be related to the method of preparation, the support surface chemistry, and the type of metal. The nitrate reduction results will be discussed in relation to these ICP results.

3.2 Catalytic reduction of nitrate

3.2.1 Catalysts prepared by method 1

3.2.1.1 Effect of support

To investigate the effect of supports on the performance of nitrate reduction catalysts, catalytic reduction experiments were performed on the following supported bimetallic catalysts prepared by method 1 (4Pd–1Cu/FCNT1,

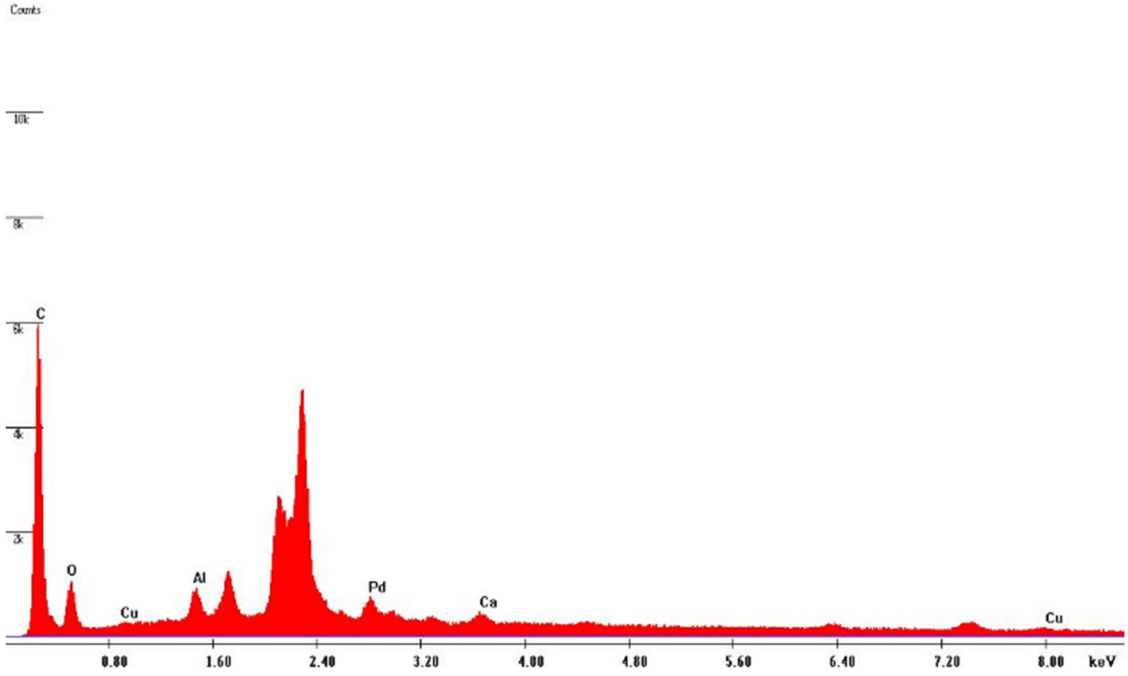

Figure 12: EDX pattern of 4Pd–1Cu/TiO_2.

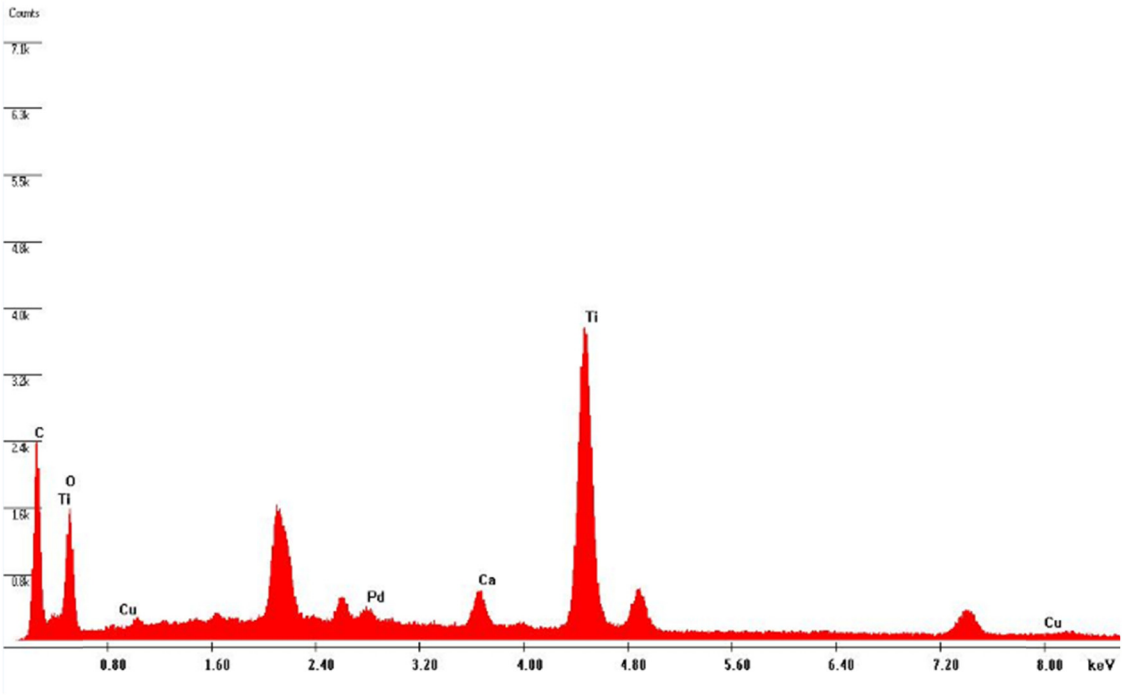

Figure 13: Nitrate conversion (%) analyzed by UV-Vis after 3 h of catalytic reduction using the supported catalysts: 4Pd–1Cu/FCNT1, 4Pd–1Cu/FCNT2, 4Pd–1Cu/AC, 4Pd–1Cu/SBA-15, and 4Pd–1Cu/TiO_2 prepared by method 1 ($C_{NO_3^-}$ = 30 ppm, $C_{catalyst}$ = 0.5 g/L).

4Pd–1Cu/FCNT2, 4Pd–1Cu/AC, 4Pd–1Cu/SBA-15, and 4Pd–1Cu/TiO_2). All experiments were carried out under the same conditions: $C_{NO_3^-}$ = 30 ppm, $C_{catalyst}$ = 0.5 g/L in absence of CO_2. The nitrate conversion levels after 3 h of reaction in the presence of the prepared catalyst analyzed by UV-Vis are shown in Figure 14. The results showed that the order of efficiency of the supported catalysts is the following: 4Pd–1Cu/TiO_2 (92%) > 4Pd–1Cu/AC (22%) = 4Pd–1Cu/$FCNT_1$ (22%) > 4Pd–1Cu/SBA-15 (4%) = 4Pd–1Cu/$FCNT_2$ (4%).

The differences in performance can be related to the surface chemistry of each support. The good properties of

Table 3: ICP results of some of the prepared catalysts

Catalyst	Palladium content (wt%)	Platinum content (wt%)	Copper content (wt%)	Tin content (wt%)
4% Pd–1% Cu/FCNT1 (Method 1)	4.15		0.43	
2% Pd–1% Cu/CNT2 (Method 1)	1.13		0.87	
2% Pd–0.6% Cu/CNT2 (Method 1)	1.05		0.59	
1% Pd–1% Cu/CNT2 (Method 1)	1.09		0.46	
2% Pd–1% Sn/CNT2 (Method 1)	1.88			0.05
2% Pt–1% Cu/CNT2 (Method 1)		0.81	0.46	
4% Pd–1% Cu/TiO_2 (Method 1)	3.47		0.84	
4% Pd–1% Cu/AC (Method 1)	4.19		0.05	
4% Pd–1% Cu/SBA-15 (Method 1)	3.96		0.9	
1% Pd–1% Cu/TiO_2 (Method 2, 200°C)	0.44		0.62	
1% Pd–1% Cu/CNT3-TiO_2 (Method 2, 200°C)	0.85		0.24	
1% Pd–1% Cu/FCNT3 (Method 2, 200°C)	0.92		0.93	
1% Pd–1% Cu/AC (Method 2, 200°C)	1.03		0.09	
1% Pd–1% Cu/SBA-15 (Method 2, 200°C)	0.85		0.89	

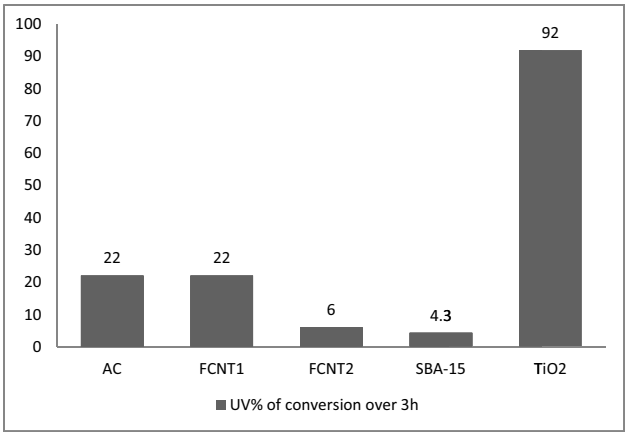

Figure 14: Nitrates conversion (%) analyzed by UV-Vis after 3 h of catalytic reduction using the supported catalysts: 2Pt–1Cu/FCNT2, 2Pd–1Sn/FCNT2, 2Pd–1Cu/FCNT2, 1Pd–1Cu/FCNT2, and 4Pd–1Cu/FCNT2 prepared by method 1 ($C_{NO_3^-}$ = 30 ppm, $C_{catalyst}$ = 0.5 g/L).

TiO_2 can be explained by the nature of the interaction between the metal nanoparticles and the TiO_2 support. Anatase TiO_2 is widely used as catalyst support for heterogeneous metal catalysts due to its strong interaction with metal nanoparticles [57]. The XRD pattern of the titanium dioxide used in this study indicates that it is 80.5% anatase. Although TiO_2 has the lowest BET surface area and lowest mesopore surface area, it exhibits higher catalytic activity than AC. This can be explained by the mechanism proposed by Sá and Anderson [27], in which nitrate adsorption occurs not only on transition metals but also on supports of bimetallic catalysts. It has been proposed that nitrate, after exchange with OH^-, adsorbs on the Lewis acid sites of TiO_2 and is reduced by the electron-rich titania species (presumably Ti_4O_7) formed by hydrogen spillover, leading to the formation of nitrite. The low conversion of nitrate by the AC-supported catalyst could be attributed to the absence of transition metal Cu as seen in ICP results. It is well known that the presence of transition metal is mandatory for the conversion of nitrate [6]. As we can see, 4Pd–1Cu/FNTC2 and 4Pd–1Cu/SBA-15 show the lowest catalytic activity although they have advantages in terms of smooth mass transfer of reactants and products during the reaction due to its mesopores structure. As we can see from S_{BET} results in Table 1, FNTC2 has a very low specific surface area, which can decrease the catalytic activity. In contrast, 4Pd–1Cu/SBA-15 has a relatively high specific surface area (686 m^2/g). The low conversion on 4Pd–1Cu/FCNT1 and 4Pd–1Cu/SBA-15 supports could be attributed to the presence of oxygen groups on their surface, which result in a high interaction between copper and O groups [58] avoiding the close contact of Cu with Pd. Thus, the reductive power is decreased as observed on oxidized CNTs in the work of Soares et al. [49]. In the presence of TiO_2-supported catalyst, the catalytic activity remains high despite the presence of hydroxyl groups due to the intervention of TiO_2 in the nitrate reduction, as we explained earlier. Moreover, the obtained results in this work are contradictory to those obtained in our previous work concerning the catalytic activity of 4Pd–1Cu/FCNT1 [59] where this latter catalyst showed the highest efficiency among the other supported catalysts (4Pd–1Cu/TiO_2, 4Pd–1Cu/AC). We should notice that the batch of CNT1 used in this work was opened 2 years before this work. Most likely, their properties have been changed or damaged with time. In addition, the production of these CNTs (CNT1) was interrupted by Sigma Aldrich for unknown reasons. Even by repeating the preparation of this catalyst in the same conditions used in the previous work, the high catalytic activity could not be obtained anymore with this support (FCNT1). Thus, this support will not be further used or discussed in this work. Soares et al. [30] have reported that CNT is effective as a catalyst support for the reduction of nitrate, which has not been verified under the conditions used in this work. We conclude that under the same conditions of preparation, the formation of active metals is achieved depending on the type of support and the metal–support interaction. Thus, the catalytic activity is related to the preparation method as well to the type of support.

3.2.1.2 Effect of metal type and loading

Catalytic reduction experiments on bimetallic catalysts prepared by method 1 and supported on FCNT2 were conducted to determine the impact of the supported metal type (2Pt–1Cu/FCNT2, 2Pd–1Sn/FCNT2, and 2Pd–1Cu/FCNT2) and metal loading (1Pd–1Cu/FCNT2 and 4Pd–1Cu/FCNT2) on the performance of the catalysts in nitrate reduction. The nitrate conversion levels after 3 h of reaction in the presence of the prepared catalysts are presented in Figure 15. All experiments were performed under the same conditions: $C_{NO_3^-}$ = 30 ppm, $C_{catalyst}$ = 0.5 g/L in absence of CO_2flow.Generally, due to the low specific surface area of CNT2 shown in Table 2 (BET), catalysts based on this support seem inactive in the reduction of nitrate, even when the loading is changing. However, by comparing the different metals tested on this support, it can be noticed that Pd–Sn supported on FCNT2 gave a slightly better conversion of nitrates.

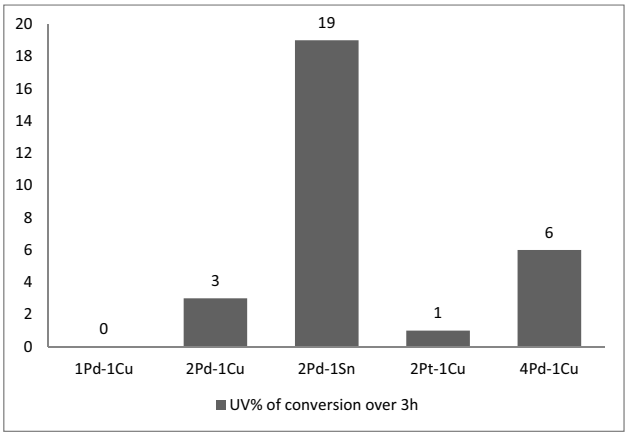

Figure 15: Nitrate conversion (%) and formed nitrites percentage (%) analyzed by IC after 2 or 3 h of catalytic reduction using the supported catalysts: 4Pd–1Cu/FCNT1, 4Pd–1Cu/FCNT2, 4Pd–1Cu/AC, 4Pd–1Cu/SBA-15, and 4Pd–1Cu/TiO_2 prepared by method 1 ($C_{NO_3^-}$ = 30 ppm, $C_{catalyst}$ = 0.5 g/L).

3.2.2 Catalysts prepared by method 2

3.2.2.1 Effect of support

a) Without CO_2 flow

To investigate the effect of supports on the performance of nitrate reduction catalysts, catalytic reduction experiments were performed on the following supported bimetallic catalysts prepared by method 2 (1Pd–1Cu/FCNT3, 1Pd–1Cu/TiO_2, and 1Pd–1Cu/CNT3-TiO_2) at 200°C. All experiments were carried out under the same conditions: $C_{NO_3^-}$ = 30 ppm, $C_{catalyst}$ = 0.5 g/L, and without CO_2 flow. The nitrate conversion levels after 3 h of reaction in the presence of the prepared catalysts analyzed by UV-Vis are shown in Table 4. The results show that 1Pd–1Cu/TiO_2 presents the highest nitrate conversion (85.5%) and 1Pd–1Cu/FNTC3 presents the lowest nitrate conversion (47%). These results are in agreement with those obtained with the catalysts prepared by method 1 and those obtained in the previous work [31], where TiO_2 showed the best catalytic activity. The catalyst supported on the composite CNT3-TiO_2 gave an intermediate conversion (78%).

Table 4: Nitrates conversion (%) analyzed by UV-Vis after 3 h of catalytic reduction using the supported catalysts: 1Pd–1Cu/FCNT3, 1Pd–1Cu/TiO_2, 1Pd–1Cu/CNT3-TiO_2, 1Pd–1Cu/SBA-15, and 1Pd–1Cu/AC prepared by method 2 at 200°C. ($C_{NO_3^-}$ = 30 ppm, $C_{catalyst}$ = 0.5 g/L)

Catalyst	Support	UV% of conv-3h
1Pd–1Cu/AC	AC	22 with CO_2
1Pd–1Cu/CNT3-TiO_2	CNT3-TiO_2	77.7 without CO_2
1Pd–1Cu/CNT3-TiO_2	CNT3-TiO_2	65.5 with CO_2
1Pd–1Cu/FCNT3	FCNT3	47 without CO_2
1Pd–1Cu/FCNT3	FCNT3	57 with CO_2
1Pd–1Cu/SBA-15	SBA-15	96 with CO_2
1Pd–1Cu/TiO_2	TiO_2	85.5 without CO_2
1Pd–1Cu/TiO_2	TiO_2	100 with CO_2

b) With CO_2 flow

The effect of supports on the performance of nitrate reduction catalyst was studied using CO_2 flow (fixed pH ≈ 5.5). Catalytic reduction experiments were performed on the following supported bimetallic catalysts, prepared by method 2 (1Pd–1Cu/FCNT3, 1Pd–1Cu/TiO_2, 1Pd–1Cu/CNT3-TiO_2, 1Pd–1Cu/SBA-15, and 1Pd–1Cu/AC) at 200°C. The nitrate conversion after 5 h of reaction in the presence of the prepared catalysts analyzed by UV-Vis is shown in Table 4. All experiments were carried out under the same conditions: $C_{NO_3^-}$ = 30 ppm, $C_{catalyst}$ = 0.5 g/L, and pH ≈ 5.5.

The order of catalyst efficiency is as follows: 1Pd–1Cu/TiO_2 (100%) > 1Pd–1Cu/SBA-15(96%) > 1Pd–1Cu/CNT3-TiO_2(66%) > 1Pd–1Cu/FCNT3 (57%) > Pd–1Cu/AC (22%). As we can see from these results, TiO_2 and SBA-15 are the most efficient supports, whereas AC showed lower activity. FCNT3 also presents a good activity, but the nitrate reduction is enhanced on the composite CNT3-TiO_2. The catalysts supported on AC and CNT have given better results in the previous works [30,31,49,60,61], and therefore, the preparation conditions used in this work are not suitable for these supports, while in the case of catalysts supported on TiO_2 or SBA-15, the result of TiO_2 is the same when comparing it with works already [15,31,62] done, but for SBA-15, there is an improvement in the percentage of nitrate conversion when comparing it with the only work done using this support in nitrate reduction [63]. The low activity in the presence of 1Pd–1Cu/AC can be explained by the absence of the transition metal Cu, as seen in ICP results. In addition, the presence of CO_2 flow seems to be effective in the nitrate reduction since the nitrate conversion increases for all the catalysts compared to the results obtained in the absence of CO_2. In general, pH fixation using CO_2 flow has a positive effect on the efficiency of catalysts in the reduction of nitrates present in water. This can be explained by the fact that nitrate reduction increases pH values to basic medium [25] (pH increases to 8 during the reaction) that could have a negative effect on the conversion of nitrates due to the anionic groups generated, which repeal the nitrate ions from the support. However, the increased catalytic activity in the acidic medium can be explained by the fact that the surface is positively charged, which favors the absorption of nitrate ions [64,65]. CO_2 is known to have an ideal buffer effect near a pH value of 5 (in this work, pH = 5.5 in the presence of CO_2) [1]. Also, the use of CO_2 reduces the

Table 5: Nitrate conversions (XNO_3^-) and nitrite, ammonium, and nitrogen selectivities (SNO_2^-, SNH_4^+, SN_2) of some of the prepared supported catalysts prepared by method 2 and reduced at 200°C at the end of the catalytic reduction ($C_{NO_3^-}$ = 30 ppm, $C_{catalyst}$ = 0.5 g/L, pH ≈ 5.5)

	t = 300 min			
Catalyst	**XNO_3^-**	**SNO_2^-**	**SNH_4^+**	**SN_2**
1Pd–1Cu/FCNT3	0.57	0.04	0.75	0.25
1Pd–1Cu/TiO_2	1.00	—	0.84	0.2
1Pd–1Cu/CNT3-TiO_2	0.65	0.00	0.21	0.79
1Pd–1Cu/SBA-15	0.96	—	0.13	0.87

formation of ammonia, which is an undesirable by-product. It is important to conclude that the surface chemistry of the support affects the formation of metals and thus the catalytic activity [66–68].

The selectivity to nitrite/ammonium/nitrogen is presented in Table 5, only for the catalysts showing a conversion percentage higher than 50. Although the selectivities should be compared at the same conversion, it was shown in the work of Soares et al. [30] that the selectivities remained practically constant after a conversion of 50%. Therefore, the selectivities at 50% conversion are compared to those at 90–100% conversion. It was observed that the catalyst 1Pd–1Cu/SBA-15 is the most selective to nitrogen, while the catalyst 1Pd–1Cu/TiO_2 is the most selective to ammonium. The catalyst supported on FCNT3 is also highly selective to ammonium. However, the selectivity to nitrogen increases in the presence of the catalyst supported by the composite CNT3-TiO_2. These results are probably related to the surface chemistry of the supports and are in agreement with the previous work [31]. It is important to note that the catalyst supported on SBA-15 has high catalytic activity as well as high nitrogen selectivity, whereas the catalyst supported on TiO_2 has high catalytic efficiency but low nitrogen selectivity.

3.2.2.2 Effect of concentration

To investigate the effect of the initial concentration of nitrates on the performance of nitrate reduction catalysts, catalytic reduction experiments were performed with two different initial concentrations of nitrates (30 ppm and 100 ppm), using the same catalyst, 1Pd–1Cu/CNT3-TiO_2, prepared by method 2 at 200°C. These two experiments were carried out under the same conditions: $C_{catalyst}$ = 0.5 g/L, with CO_2 flow (pH ≈ 5.5). The results of the conversion using the same catalyst were affected by the starting nitrate concentration. When the same catalyst was used, at a higher initial nitrate concentration of 100 ppm, the conversion of nitrates was 74%, while at a lower initial nitrate concentration of 30 ppm, it reduced to 65.5%.

3.2.2.3 Effect of the preparation method

The effect of the preparation method on the performance of nitrate reduction catalysts was studied in the catalytic reduction experiments using catalysts prepared by methods 1 and 2. The nitrate conversion levels after 3 h of reaction with each of the catalysts are shown in Tables 4 and 5. The result shows us that all the catalysts prepared by method 2 have a higher catalytic activity in the reduction of nitrates, than those prepared by method 1 which seems inactive. We can conclude that $NaBH_4$ used as a reducing agent is not the best choice to reduce the precursor salts when CNTs or SBA-15 are used as supports. This may be due to the fact that CNTs and SBA-15 have a large number of O groups that interact with copper, avoiding the close contact between Cu and Pd, which decreases the reducing power, and thus, the thermal reduction under hydrogen will be more effective in reducing the precursor metals since the temperature decomposes some of the oxygenated groups and since H_2 reduces CuO at appropriate temperatures [30]. It is important to notice that method 1 was effective when TiO_2 was used as support. Thus, the formation of active metals and their catalytic activity depend on the support surface chemistry, which affects the metal–support interaction.

3.2.3 Kinetic study

The nitrate conversion levels and the formed nitrites percentage during 3 h of reaction with the following supports prepared by method 1 (4Pd–1Cu/FCNT1, 4Pd–1Cu/FCNT2, 4Pd–1Cu/AC, 4Pd–1Cu/SBA-15, and 4Pd–1Cu/TiO_2) analyzed by ionic chromatography (IC) are shown in Figure 16. The outcomes are nearly identical to those of the UV analysis, where the catalyst supported by TiO_2 had the highest conversion of nitrates (100%) with a very rapid increase in the conversion during the first 30 minutes. The concentration of nitrites, however, is still high even at the end of the reaction (after 2 hours), indicating that nitrites in this case are not transformed into final products (N_2 or NH_4^+) despite the significant conversion of nitrates. The nitrate conversion levels and the formed nitrites percentage during 3 h of reaction with each one of the supported catalysts (1Pd–1Cu/FCNT3, 1Pd–1Cu/TiO_2, and 1Pd–1Cu/CNT3-TiO_2) prepared

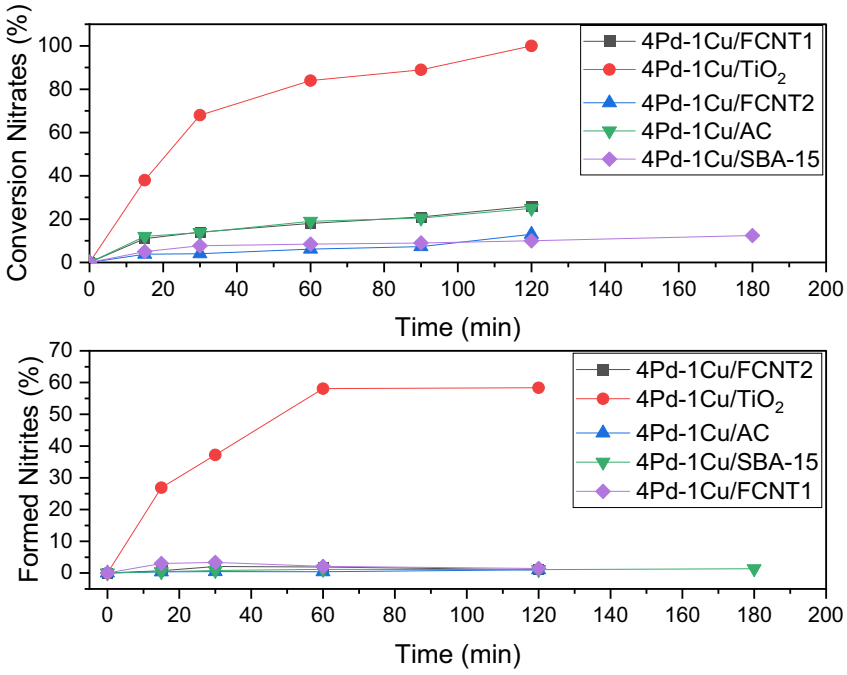

Figure 16: Nitrate conversion (%) and formed nitrites percentage (%) analyzed by IC after 3 h or 5 h of catalytic reduction using the supported catalysts: 1Pd–1Cu/FCNT3, 1Pd–1Cu/TiO_2, and 1Pd–1Cu/CNT3-TiO_2 prepared by method 2 with and without CO_2 flow ($C_{NO_3^-}$ = 30 ppm, $C_{catalyst}$ = 0.5 g/L).

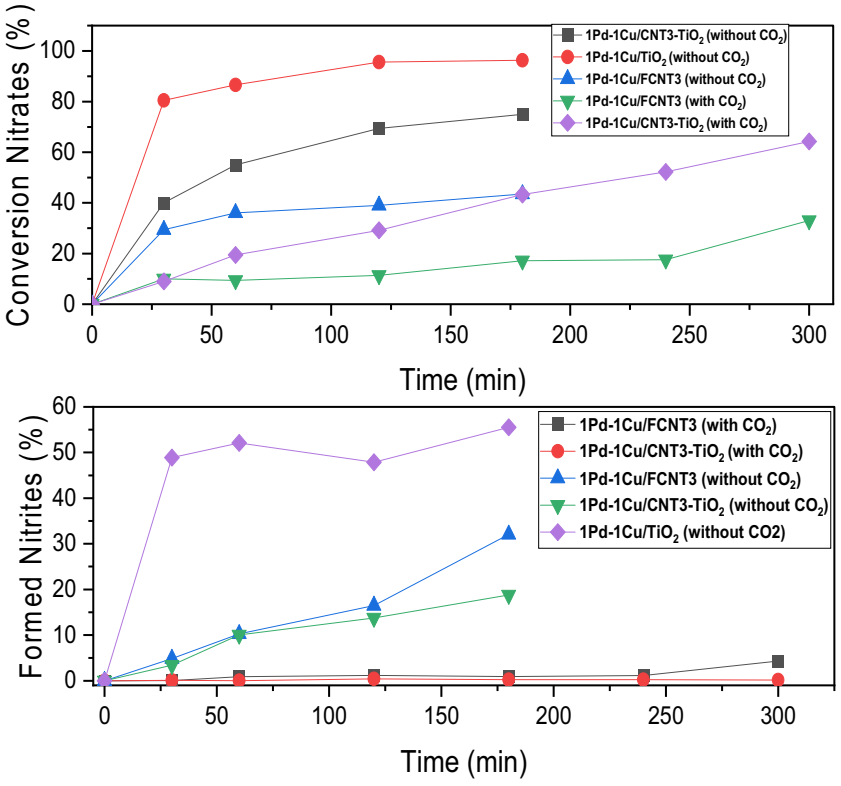

Figure 17: EDX pattern of 4Pd–1Cu/CNT2.

by method 2 tested with or without CO_2 flow and analyzed by IC are shown in Figure 17. The results of the nitrate conversion are similar to those analyzed by the UV spectrophotometer. Results from a catalyst test that involved converting nitrates and forming nitrites over the course of a 3-hour reaction period showed the following: during the first 30 minutes, there is a rapid increase in nitrate conversion; after that, the conversion rises gradually during the remainder of the reaction. Second, the percentage of generated nitrite is reduced but still high in the cases of 1Pd–1Cu/CNT3-TiO_2 and 1Pd–1Cu/FCNT3 catalysts. Nitrite created in the presence of the 1Pd–1Cu/TiO_2 catalyst had the greatest percentage throughout the process and continued to form until the completion of the reaction (after 3 h). In the absence of CO_2 flow, we conclude that nitrite is the end result of nitrate reduction. We can see that the conversion of the two supported catalysts, FCNT3 and CNT3-TiO_2, tested with CO_2 flow increases slowly with time until the end of the reaction after 5 h. According to Figure 11, we can notice that the concentration of nitrite is low during the reaction in the case of two catalysts, and this is explained by the continuous transformation of nitrite into the final product (N_2 or NH_4^-) which is not observed in the absence of CO_2 flow in the same figure. Thus, we conclude that the presence of CO_2 helps to decrease the nitrite concentration during the nitrate reduction.

4 Conclusions

In this study, we tested bimetallic catalysts based on different supports by changing the metals deposited, the methods of preparation of catalysts and the reaction conditions to study the effect of all these parameters on the efficiency of catalysts, and to choose the best catalyst in the reduction of nitrates in terms of efficiency and selectivity toward nitrogen in the best reaction conditions. The results obtained showed that SBA-15 is a suitable supported catalyst for nitrate reduction where complete conversion of nitrate is obtained for 4Pd–1Cu/SBA-15 reduced with H_2 at 100°C and 96% conversion for 1Pd–1Cu/SBA-15 reduced with H_2 at 200°C and the highest selectivity toward nitrogen (87%) when compared with other supported catalysts. In spite of the total conversion of nitrates using the supported catalysts on TiO_2 whatever the method of preparation, the high selectivity shown by these catalysts toward ammonium is a great disadvantage because they solve a problem on the one hand and create a greater problem in terms of toxicity on the other hand. In general, the catalytic activity and selectivity toward nitrogen or ammonium depend on the many factors such as the support type, the metal type, the preparation method, the reduction temperature of the catalysts, and the experimental conditions of nitrate reduction. It has been observed that the preparation of the catalysts with H_2 at high temperature allows the formation of active metals and thus improves the efficiency of these supported catalysts in nitrate conversion. The pH fixation using CO_2 flow improved the efficiency of supported catalysts except in the case of CNT-TiO_2 composite. The mesoporous silica SBA-15 is a very suitable catalyst support for nitrate reduction in terms of catalytic activity and selectivity to nitrogen. This opens up new opportunities in the development of new supported catalysts to improve the catalytic activity and selectivity for nitrogen in nitrate reduction. However, optimization of catalyst N_2 selectivity, activity, and lifetime is still needed before catalytic reduction can be implemented as a full-scale method for effective water treatment.

Funding information: No funding for this research work

Author contributions: Mouhamad Rachini: investigation, methodology, and writing–original draft; Mira Jaafar: formal analysis, writing – review, methodology, and supervision; Nabil Tabaja: formal analysis, methodology, and writing – review; Sami Tlais: methodology and writing – review; Rasha Hamdan: methodology and writing – review; Fatima Al Ali: formal analysis and methodology; Ola Haidar: investigation; Christine Lancelot: investigation and methodology; Mohammad Kassem: supervision, methodology, and writing – review; Eugene Bychkov: supervision; Lucette Tidahy: methodology and validation; Renaud Cousin: formal analysis and conceptualization; Dorothée Dewaele: methodology and validation; Tayssir Hamieh: supervision, resources, and writing – review and editing; Joumana Toufaily: supervision, conceptualization, and project management.

Conflict of interest: The authors state no conflict of interests.

Ethical approval: The conduct research is not related to either human or animal use.

Data availability statement: The datasets generated during and/or analyzed during the current study are available from the corresponding author on reasonable request.

References

[1] Centi G, Perathoner S. Remediation of water contamination using catalytic technologies. Appl Catal B: Environ. 2003;41(1–2):15–29. doi: 10.1016/S0926-3373(02)00198-4.

[2] Riedel B, Pados T, Pretterebner K, Schiemer L, Steckbauer A, Haselmair A, et al. Effect of hypoxia and anoxia on invertebrate behaviour: Ecological perspectives from species to community level. Biogeosciences. 2014;11(6):1491–1518. doi: 10.5194/bg-11-1491-2014.

[3] Hörold S, Vorlop K-D, Tacke T, Sell M. Development of catalysts for a selective nitrate and nitrite removal from drinking water. Catal Today. 1993;17(1–2):21–30. doi: 10.1016/0920-5861(93)80004-K.

[4] Kapoor A, Viraraghavan T. Nitrate removal from drinking water–review. J Environ Eng. 1997;123(4):371–80. doi: 10.1061/(ASCE)0733-9372(1997)123:4(371).

[5] Vorlop KD, Tacke T. 1st steps towards noble-metal catalyzed removal of nitrate and nitrite from drinking-water. Chem Ing Tech. 1989;61:836–7.

[6] Huang YH, Zhang TC. Effects of dissolved oxygen on formation of corrosion products and concomitant oxygen and nitrate reduction in zero-valent iron systems with or without aqueous Fe2 +. Water Res. 2005;39(9):1751–60. doi: 10.1016/j.watres.2005.03.002.

[7] Jensen VB, Darby JL, Seidel C, Gorman C. Nitrate in potable water supplies: Alternative management strategies. Crit Rev Environ Sci Technol. 2014;44(20):2203–86. doi: 10.1080/10643389.2013.828272.

[8] Matějů V, Čižinská S, Krejčí J, Janoch T. Biological water denitrification–a review. Enzyme Microb Technol. 1992;14(3):170–83. doi: 10.1016/0141-0229(92)90062-S.

[9] Moreno B, Gómez MA, González-López J, Hontoria E. Inoculation of a submerged filter for biological denitrification of nitrate polluted groundwater: A comparative study. J Hazard Mater. 2005;117(2–3):141–7. doi: 10.1016/j.jhazmat.2004.09.027.

[10] Hamid S, Bae S, Lee W, Amin MT, Alazba AA. Catalytic nitrate removal in continuous bimetallic Cu–Pd/Nanoscale zerovalent iron system. Ind Eng Chem Res. 2015;54(24):6247–57. doi: 10.1021/acs.iecr.5b01127.

[11] Ruiz-Beviá F, Fernández-Torres MJ. Effective catalytic removal of nitrates from drinking water: An unresolved problem? J Clean Prod. 2019;217:398–408. doi: 10.1016/j.jclepro.2019.01.261.

[12] Jung S, Bae S, Lee W. Development of Pd–Cu/Hematite catalyst for selective nitrate reduction. Env Sci Technol. 2014;48(16):9651–8. doi: 10.1021/es502263p.

[13] Prüsse U, Vorlop K-D. Supported bimetallic palladium catalysts for water-phase nitrate reduction. J Mol Catal A: Chem. 2001;173(1–2):313–28. doi: 10.1016/S1381-1169(01)00156-X.

[14] Martínez J, Ortiz A, Ortiz I. State-of-the-art and perspectives of the catalytic and electrocatalytic reduction of aqueous nitrates. Appl Catal B: Environ. 2017;207:42–59. doi: 10.1016/j.apcatb.2017.02.016.

[15] Gao W, Guan N, Chen J, Guan X, Jin R, Zeng H, et al. Titania supported Pd-Cu bimetallic catalyst for the reduction of nitrate in drinking water. Appl Catal B: Environ. 2003;46(2):341–51. doi: 10.1016/S0926-3373(03)00226-1.

[16] Deganello F, Liotta LF, Macaluso A, Venezia AM, Deganello G. Catalytic reduction of nitrates and nitrites in water solution on pumice-supported Pd–Cu catalysts. Appl Catal B: Environ. 2000;24(3–4):265–73. doi: 10.1016/S0926-3373(99)00109-5.

[17] Ilinitch OM, Cuperus FP, Nosova LV, Gribov EN. Catalytic membrane in reduction of aqueous nitrates: Operational principles and catalytic performance. Catal Today. 2000;56(1–3):137–45. doi: 10.1016/S0920-5861(99)00270-9.

[18] Epron F, Gauthard F, Pinéda C, Barbier J. Catalytic reduction of nitrate and nitrite on Pt–Cu/Al2O3 catalysts in aqueous solution: Role of the interaction between copper and platinum in the reaction. J Catal. 2001;198(2):309–18. doi: 10.1006/jcat.2000.3138.

[19] Gauthard F. Palladium and platinum-based catalysts in the catalytic reduction of nitrate in water: Effect of copper, silver, or gold addition. J Catal. 2003;220(1):182–91. doi: 10.1016/S0021-9517(03)00252-5.

[20] Lemaignen L, Tong C, Begon V, Burch R, Chadwick D. Catalytic denitrification of water with palladium-based catalysts supported on activated carbons. Catal Today. 2002;75(1–4):43–8. doi: 10.1016/S0920-5861(02)00042-1.

[21] Mikami I, Sakamoto Y, Yoshinaga Y, Okuhara T. Kinetic and adsorption studies on the hydrogenation of nitrate and nitrite in water using Pd-Cu on active carbon support. Appl Catal B: Environ. 2003;44(1):79–86. doi: 10.1016/S0926-3373(03)00021-3.

[22] Sá J, Vinek H. Catalytic hydrogenation of nitrates in water over a bimetallic catalyst. Appl Catal B: Environ. 2005;57(4):247–56. doi: 10.1016/j.apcatb.2004.10.019.

[23] Pintar A, Batista J, Levec J. Catalytic denitrification: Direct and indirect removal of nitrates from potable water. Catal Today. 2001;66(2):503–10. doi: 10.1016/S0920-5861(00)00622-2.

[24] Sá J, Gasparovicova; D, Hayek K, Halwax E, Anderson JA, Vinek H. Water Denitration over a Pd–Sn/Al_2O_3 Catalyst. Catal Lett. 2005;105:209–17. doi: 10.1007/s10562-005-8692-7.

[25] Garron A, Lázár K, Epron F. Effect of the support on tin distribution in Pd–Sn/Al2O3 and Pd–Sn/SiO2 catalysts for application in water denitration. Appl Catal B: Environ. 2005;59(1–2):57–69. doi: 10.1016/j.apcatb.2005.01.002.

[26] Marchesini FA, Picard N, Miró EE. Study of the interactions of Pd,In with SiO2 and Al2O3 mixed supports as catalysts for the hydrogenation of nitrates in water. Catal Commun. 2012;21:9–13. doi: 10.1016/j.catcom.2012.01.015.

[27] Sá J, Anderson JA. FTIR study of aqueous nitrate reduction over Pd/TiO2. Appl Catal B: Environ. 2008;77(3–4):409–17. doi: 10.1016/j.apcatb.2007.08.013.

[28] Sakamoto Y, Kamiya Y, Okuhara T. Selective hydrogenation of nitrate to nitrite in water over Cu-Pd bimetallic clusters supported on active carbon. J Mol Catal A: Chem. 2006;250(1–2):80–6. doi: 10.1016/j.molcata.2006.01.041.

[29] Catalytic reduction of nitrate on Pt-Cu and Pd-Cu on active carbon using continuous reactor: The effect of copper nanoparticles - ScienceDirect. https://www.sciencedirect.com/science/article/pii/S0926337305002730 (accessed 2023-02-04).

[30] Soares OSGP, Órfão JJM, Pereira MFR. Pd–Cu and Pt–Cu catalysts supported on carbon nanotubes for nitrate reduction in water. Ind Eng Chem Res. 2010;49(16):7183–92. doi: 10.1021/ie1001907.

[31] Soares OSGP, Órfão JJM, Pereira MFR. Nitrate reduction in water catalysed by Pd–Cu on different supports. Desalination. 2011;279(1–3):367–74. doi: 10.1016/j.desal.2011.06.037.
[32] Sa J, Berger T, Fottinger K, Riss A, Anderson J, Vinek H. Can TiO2 promote the reduction of nitrates in water? J Catal. 2005;234(2):282–91. doi: 10.1016/j.jcat.2005.06.015.
[33] Nitrate removal in drinking waters: the effect of tin oxides in the catalytic hydrogenation of nitrate by Pd/SnO2 catalysts - ScienceDirect. https://www.sciencedirect.com/science/article/pii/S0926337302000322 (accessed 2023-02-04).
[34] Supported Pd–Cu catalysts in the water phase reduction of nitrates: Functional resin versus alumina - ScienceDirect. https://www.sciencedirect.com/science/article/pii/S1381116906011897 (accessed 2023-02-04).
[35] Catalytic Hydrogenation of Aqueous Nitrate over Pd–Cu/ZrO2 Catalysts | Industrial & Engineering Chemistry Research. https://pubs.acs.org/doi/10.1021/ie9005854 (accessed 2023-02-04).
[36] Use of palladium based catalysts in the hydrogenation of nitrates in drinking water: from powders to membranes - ScienceDirect. https://www.sciencedirect.com/science/article/pii/S0920586199002333 (accessed 2023-02-04).
[37] Yoshinaga Y, Akita T, Mikami I, Okuhara T. Hydrogenation of nitrate in water to nitrogen over Pd–Cu supported on active carbon. J Catal. 2002;207(1):37–45. doi: 10.1006/jcat.2002.3529.
[38] Sanchis Pérez I, Díaz Nieto E, Pizarro AH, Rodriguez JJ, Mohedano AF. Nitrate reduction with bimetallic catalysts. A Stability-Addressed Overv. Sep Purif Technol. 2022;290:120750. doi: 10.1016/j.seppur.2022.120750.
[39] Gao B, Chen GZ, Li Puma G. Carbon nanotubes/titanium dioxide (CNTs/TiO2) nanocomposites prepared by conventional and novel surfactant wrapping sol–gel methods exhibiting enhanced photocatalytic activity. Appl Catal B: Environ. 2009;89(3–4):503–9. doi: 10.1016/j.apcatb.2009.01.009.
[40] Saleh TA. The influence of treatment temperature on the acidity of MWCNT oxidized by HNO3 or a mixture of HNO3/H2SO4. Appl Surf Sci. 2011;257(17):7746–51. doi: 10.1016/j.apsusc.2011.04.020.
[41] Li C, Zhang Q, Wang Y, Wan H. Preparation, characterization and catalytic activity of palladium nanoparticles encapsulated in SBA-15. Catal Lett. 2008;120(1–2):126–36. doi: 10.1007/s10562-007-9263-x.
[42] Ganiyu SA, Tanimu A, Azeez MO, Alhooshani K. Hierarchical porous nitrogen-doped carbon modified with nickel nanoparticles for selective ultradeep desulfurization. ChemistrySelect. 2020;5(28):8483–93. doi: 10.1002/slct.202000921.
[43] Naoe K, Kataoka M, Kawagoe M. Preparation of water-soluble palladium nanocrystals by reverse micelle method: Digestive ripening behavior of mercaptocarboxylic acids as stabilizing agent. Colloids Surf A: Physicochemical Eng Asp. 2010;364(1–3):116–22. doi: 10.1016/j.colsurfa.2010.05.004.
[44] Astuti Y, Hartinah S, Darmawan A, Widiyandari H. Synthesis and characterization of bismuth oxide/commercial activated carbon composite for battery anode. Open Chem. 2022;20(1):1476–84. doi: 10.1515/chem-2022-0247.
[45] Nasralla N, Yeganeh M, Astuti Y, Piticharoenphun S, Shahtahmasebi N, Kompany A, et al. Structural and spectroscopic study of Fe-doped TiO2 nanoparticles prepared by sol–gel method. Sci Iran. 2013;20(3):1018–22. doi: 10.1016/j.scient.2013.05.017.
[46] Nasralla NHS, Yeganeh M, Astuti Y, Piticharoenphun S, Šiller L. Systematic study of electronic properties of Fe-doped TiO2 nanoparticles by X-Ray photoemission spectroscopy. J Mater Sci: Mater Electron. 2018;29(20):17956–66. doi: 10.1007/s10854-018-9911-5.
[47] Darmawan A, Rasyid SA, Astuti Y. Modification of the glass surface with hydrophobic silica thin layers using tetraethylorthosilicate (TEOS) and trimethylchlorosilane (TMCS) precursors. Surf Interface Anal. 2021;53(3):305–13. doi: 10.1002/sia.6917.
[48] Yan W, Chen B, Mahurin SM, Schwartz V, Mullins DR, Lupini AR, et al. Preparation and comparison of supported gold nanocatalysts on anatase, brookite, rutile, and P25 polymorphs of TiO_2 for catalytic oxidation of CO. J Phys Chem B. 2005;109(21):10676–85. doi: 10.1021/jp044091o.
[49] Soares OSGP, Órfão JJM, Pereira MFR. Bimetallic catalysts supported on activated carbon for the nitrate reduction in water: Optimization of catalysts composition. Appl Catal B: Environ. 2009;91(1–2):441–8. doi: 10.1016/j.apcatb.2009.06.013.
[50] Nakada Y, Aksenov I, Okumura H. Scanning tunneling microscopy studies of formation of 8×5 reconstructed structure of Ga on the Si(001) surface. J Vac Sci Technol B. 1999;17(1):1. doi: 10.1116/1.590509.
[51] Tao Y, Endo M, Ohsawa R, Kanoh H, Kaneko K. High capacitance carbon-based xerogel film produced without critical drying. Appl Phys Lett. 2008;93(19):193112. doi: 10.1063/1.2976684.
[52] Sing KSW. Reporting physisorption data for gas/solid systems with special reference to the determination of surface area and porosity (Provisional). Pure Appl Chem. 1982;54(11):2201–18. doi: 10.1351/pac198254112201.
[53] Parida KM, Rath D. Structural properties and catalytic oxidation of benzene to phenol over CuO-impregnated mesoporous silica. Appl Catal A: Gen. 2007;321(2):101–8. doi: 10.1016/j.apcata.2007.01.054.
[54] Batista J, Pintar A, Mandrino D, Jenko M, Martin V. XPS and TPR examinations of γ-Alumina-Supported Pd-Cu catalysts. Appl Catal A: Gen. 2001;206(1):113–24. doi: 10.1016/S0926-860X(00)00589-5.
[55] Gurrath M, Kuretzky T, Boehm HP, Okhlopkova LB, Lisitsyn AS, Likholobov VA. Palladium catalysts on activated carbon supports. Carbon. 2000;38(8):1241–55. doi: 10.1016/S0008-6223(00)00026-9.
[56] Mendez CM, Olivero H, Damiani DE, Volpe MA. On the role of Pd β-Hydride in the reduction of nitrate over Pd based catalyst. Appl Catal B: Environ. 2008;84(1–2):156–61. doi: 10.1016/j.apcatb.2008.03.019.
[57] Bagheri S, Shameli K, Abd Hamid SB. Synthesis and characterization of anatase titanium dioxide nanoparticles using egg white solution via sol-gel method. J Chem. 2013;2013:1–5. doi: 10.1155/2013/848205.
[58] Effect of Activated Carbon Surface Oxygen- and/or Nitrogen-Containing Groups on Adsorption of Copper(II) Ions from Aqueous Solution | Langmuir. https://pubs.acs.org/doi/pdf/10.1021/la9815704 (accessed 2022-09-14).
[59] Laboratory of Materials, Catalysis, Environment and Analytical Methods (MCEMA), EDST, FS, Lebanese University, P.O. Box 11-2806, Hariri Campus, Hadath, Lebanon; M. Rachini, Pd-Cu

bimetallic based catalysts for nitrate remediation in water: synthesis, characterization, and the influence of supports. CR. 2022;2(2):1. doi: 10.21926/cr.2202011.
[60] Soares OSGP, Órfão JJM, Pereira MFR. Activated carbon supported metal catalysts for nitrate and nitrite reduction in water. Catal Lett. 2008;126(3–4):253–60. doi: 10.1007/s10562-008-9612-4.
[61] Matatov-Meytal U, Sheintuch M. Activated carbon cloth-supported Pd–Cu catalyst: Application for continuous water denitrification. Catal Today. 2005;102–103:121–7. doi: 10.1016/j.cattod.2005.02.015.
[62] Bagheri S, Muhd Julkapli N, Bee Abd Hamid S. Titanium dioxide as a catalyst support in heterogeneous catalysis. Sci World J. 2014;2014:1–21. doi: 10.1155/2014/727496.
[63] Min-Sung K, Sang-Ho C, Myung Suk L, Dae-Won L, Kwan-Young L. Catalytic nitrate reduction in water over mesoporous silica supported Pd-Cu catalysts. Clean Technol. 2013;19(1):65–72. doi: 10.7464/KSCT.2013.19.1.065.
[64] Soares OSGP, Órfão JJM, Ruiz-Martínez J, Silvestre-Albero J, Sepúlveda-Escribano A, Pereira MFR. Pd–Cu/AC and Pt–Cu/AC catalysts for nitrate reduction with hydrogen: Influence of calcination and reduction temperatures. Chem Eng J. 2010;165(1):78–88. doi: 10.1016/j.cej.2010.08.065.
[65] Gao Y, Liu H, Ma M. Preparation and photocatalytic behavior of TiO2-carbon nanotube hybrid catalyst for acridine dye decomposition. React Kinet Catal Lett. 2007;90(1):11–8. doi: 10.1007/s11144-007-4884-z.
[66] Somorjai GA, Li Y. Impact of surface chemistry. Proc Natl Acad Sci. 2011;108(3):917–24. doi: 10.1073/pnas.1006669107.
[67] Supported Metal Catalyst - an overview | ScienceDirect Topics. https://www.sciencedirect.com/topics/engineering/supported-metal-catalyst (accessed 2022-09-28).
[68] Barbir F. CHAPTER 4 - Main cell components, materials properties and processes. In: Barbir F, editor. PEM Fuel Cells. Burlington: Academic Press; 2005. p. 73–113. doi: 10.1016/B978-012078142-3/50005-7.